How focused pumping affects type-II spontaneous parametric down-conversion

Lee, P.S.K.; Exter, M.P. van; Woerdman, J.P.

How focused pumping affects type-II spontaneous parametric down-conversion

P. S. K. Lee, M. P. van Exter, and J. P. Woerdman
Huygens Laboratory, Leiden University, P. O. Box 9504, 2300 RA Leiden, The Netherlands
(Received 25 April 2005; published 8 September 2005)

We demonstrate that the transition from plane-wave to focused pumping in type-II down-conversion is analogous to the transition from cw to pulsed pumping. We show experimentally that focused pumping leads to asymmetric broadening of both the ordinary and extraordinary light distribution. It hardly affects the entanglement quality if proper spatial filtering is applied.

DOI: 10.1103/PhysRevA.72.033803 PACS number(s): 42.65.Lm, 42.50.Dv

I. INTRODUCTION

Spontaneous parametric down-conversion (SPDC) has become the common method to generate entangled photon pairs for experimental studies on fundamental features of quantum mechanics [1–3]. Though these photon pairs can be simultaneously entangled in energy, momentum, and polarization (for type-II SPDC), the use of polarization entanglement is most popular due to its simplicity. The general theoretical aspects of two-photon entanglement in type-II SPDC are well known and thoroughly studied in [4,5]. More specifically, also the effect of the *spectral* properties of the pump on the down-converted light has been the topic of investigation in several papers, including the effect of the spectral pump width on the spatial coherence of the down-converted beams [6] and the spectral consequences of broadband pulsed [7,8] pumping in type-II SPDC.

The role of the *spatial* properties of the pump in type-II SPDC, and particularly that of focused pumping [9,10], is a less explored regime, though. Proper focusing of the pump laser is certainly necessary when the entangled photon pairs are detected with fiber-coupled photon counters [11,12]. In order to optimize the collection of entangled photon pairs, both the size of the backward-propagated fiber mode and the transverse beam walk-off in the crystal have to match the size of the pump spot [11]. A potentially beneficial effect of focused pumping may also arise when using "bucket" detectors behind apertures for pair detection. A simple argument that suggests such effect is that the large wave-vector spread associated with focused pumping will generally broaden the two rings that comprise the usual SPDC pattern. The increased area of the ring crossings might thus allow us to work with larger apertures and enhance the yield of polarization-entangled photon pairs. To investigate the feasibility of this scheme and check for any side effects in both the bucket and fiber-coupled detection scheme, a better understanding of the role of focused pumping in SPDC is needed.

In this paper, we study the effect of focused pumping on the single-photon image generated via type-II SPDC, contrary to papers that specifically treat the effect on coincidence imaging [9,10]. In particular, we theoretically and experimentally demonstrate that the transition from plane-wave to focused pumping leads to the same *asymmetric* broadening of both down-converted rings. Our theoretical description follows the approach that Grice and Walmsley [8] use to analyze the difference between the ordinary and extraordinary spectrum in the transition from cw pumping to broadband (pulsed) pumping, which could be loosely called "the effects of focusing in time" (instead of space). We also study the consequences of focused pumping for the measured photon yield and entanglement quality of the polarization-entangled photon pairs. We present the experimental data that support these consequences for bucket detection only and include the case of fiber-coupled detection in an outlook discussion.

II. THEORY

In this section we present an analysis of the spatial properties of photons generated via type-II SPDC under focused pumping. Grice and Walmsley [8] have analyzed the spectral properties of the generated ordinary (o) and extraordinary (e) photons at fixed transverse momentum $\mathbf{q}_o=\mathbf{q}_e=\mathbf{0}$ and plane-wave pumping by expressing the spectral SPDC profile as a frequency integral of the pump envelope function and phase matching function. We perform a similar integration in space to analyze the complementary problem, i.e., calculating the SPDC emission profile for cw pumping at fixed frequency ($\omega_o \approx \omega_e \approx \omega_p/2 \equiv \Omega$). The angular-emission profile for this case is then represented by the differential single-photon count rate (per angular and frequency bandwidth) which, for the o-polarized emission, can be expressed as

$$\frac{dR_o}{d\boldsymbol{\theta}_o d\omega_o} \propto \int d\boldsymbol{\theta}_e I(\boldsymbol{\theta}_p)\mathrm{sinc}^2[\phi(\boldsymbol{\theta}_e,\boldsymbol{\theta}_o)], \tag{1}$$

where $I(\boldsymbol{\theta}_p)=\int d\omega_p |E_p(\boldsymbol{\theta}_p;\omega_p)|^2$ is the pump envelope function, expressed in the pump angle $\boldsymbol{\theta}_p \approx (c/\omega_p)\mathbf{q}_p$. Conservation of each component of the pump transverse momentum $\mathbf{q}_p$ requires $\mathbf{q}_p=\mathbf{q}_o+\mathbf{q}_e$ or, equivalently, $2\boldsymbol{\theta}_p=\boldsymbol{\theta}_o+\boldsymbol{\theta}_e$. The phase mismatch $\phi=\Delta k_z L/2$ built up during propagation over half the crystal length L is incorporated in the function $\mathrm{sinc}(x)\equiv \sin(x)/x$. The emission profile for the e-polarized photons is obtained by swapping the o and e indices in Eq. (1).

The solution of the angular integral Eq. (1) is more difficult than that of the frequency integral encountered in Ref. [8]. The reason is not so much the increase from one to two dimensions, but rather the more complicated structure of the phase-mismatch function ϕ, which is at least quadratic in the

transverse momenta. To keep the expressions manageable we will only consider the case of mild focusing, where the angular profile of the pump is much smaller than the angular radii of the generated SPDC rings. Whenever possible we will also neglect the small differences between the various refractive indices (denoted by a single parameter n) and take the internal walk-off angle of the e-polarized pump and SPDC light identical as $\rho=(2/n)\theta_{\mathrm{off}}$. Under these conditions, the phase mismatch becomes [13,14]

$$\phi(\boldsymbol{\theta}_p,\boldsymbol{\theta}_o,\boldsymbol{\theta}_e)\approx\left(\frac{L\Omega}{2c}\right)\left(-C+\rho(2\theta_{p,y}-\theta_{e,y})+\frac{1}{2n}(\theta_{o,x}^2+\theta_{o,y}^2+\theta_{e,x}^2+\theta_{e,y}^2)\right), \tag{2}$$

where C is a constant that depends on material properties and cutting angle, where all external angles $|\boldsymbol{\theta}_i|\ll 1$ are measured with respect to the (z-directed) surface normal, and where the c axis of the uniaxial crystal lies in the yz plane. Equation (2) highlights the phase-matching physics: the two linear terms arise from the angle dependence of the extraordinary refractive index (for both pump and e ray), while the second-order terms arise from the reduction in k_z at non-normal incidence (second-order terms in θ_p are neglected). The angular shape of the o-polarized emission is found by removing $\boldsymbol{\theta}_e\equiv(\theta_{e,x},\theta_{e,y})$ from Eq. (2) which gives

$$\phi(\boldsymbol{\theta}_p,\boldsymbol{\theta}_o)=\left(\frac{L\Omega}{2nc}\right)[|\boldsymbol{\theta}_o+\theta_{\mathrm{off}}\mathbf{e}_y-\boldsymbol{\theta}_p|^2-(\theta_{\mathrm{off}}\sqrt{2}-\theta_{p,y}/\sqrt{2})^2], \tag{3}$$

for $C=\theta_{\mathrm{off}}^2/n$, and vice versa for the e profile.

For plane-wave pumping, the emission profiles are completely determined by the phase-matching condition $\phi\approx 0$. The two polarized components are emitted in angular cones (=rings in the far field) that are approximate mirror images of each other and are vertically displaced with respect to the pump over angles $-\theta_{\mathrm{off}}$ and θ_{off}, for the o and e rays, respectively [5]. From Eq. (3) we can see that, for the chosen constant C, these rings have radii $\theta_r=\theta_{\mathrm{off}}\sqrt{2}$ and cross each other at 90° if the pump enters at normal incidence ($\boldsymbol{\theta}_p=\mathbf{0}$). For plane-wave pumping at non-normal incidence, angle tuning in the x direction will produce a simple x shift of the SPDC pattern, whereas angle tuning in the y direction produces a y shift as well as a change in the ring radii [see Eq. (3) and Fig. 1]. By combining these effects in the integration over the angular pump profile we can explain the asymmetric angular smearing observed under focused pumping.

For the visual picture of the asymmetric broadening, we introduce (shifted) radial coordinates $\theta_r+\delta\theta_r$ and φ (see Fig. 1), which are defined by $\theta_x=(\theta_r+\delta\theta_r)\cos\varphi$ and $\theta_y=(\theta_r+\delta\theta_r)\sin\varphi\pm\theta_{\mathrm{off}}$ (the plus and minus signs apply to the e and o rings, respectively). By implementing these radial coordinates in Eq. (3) we can write Eq. (1) as

$$\frac{dR_o}{d\boldsymbol{\theta}_o d\omega_o}\propto\int d\boldsymbol{\theta}_p\exp(-2|\boldsymbol{\theta}_p|^2/\sigma^2)\mathrm{sinc}^2\times\{\pi[\delta\theta_r-\mathbf{a}(\varphi)\cdot\boldsymbol{\theta}_p]/\bar{\theta}\}, \tag{4}$$

where $\bar{\theta}=\pi nc/(L\Omega\theta_r)$ is the radial width of the SPDC ring for plane-wave pumping and $I(\boldsymbol{\theta}_p)=\exp(-2|\boldsymbol{\theta}_p|^2/\sigma^2)$ is the Gaussian pump envelope function with pump divergence σ. This expression determines the asymmetric ring smearing under focused pumping via the vector $\mathbf{a}(\varphi)=(\cos\varphi,1/\sqrt{2}-\sin\varphi)$, which quantifies the "local changes in ring radius" induced by the spread in $\boldsymbol{\theta}_p$. For a more direct insight into the ring smearing, it is useful to decompose the pump angle $\boldsymbol{\theta}_p$ into components perpendicular ($\theta_{p\perp}$) and parallel ($\theta_{p\parallel}$) to $\mathbf{a}(\varphi)$. As only the component $\theta_{p\parallel}$ contributes to the phase mismatch, we can easily remove the Gaussian integral over $\theta_{p\perp}$ and reduce Eq. (4) to a one-dimensional integral. The only relevant parameter in this integral is the dimensionless ratio $x(\varphi)$ between the projected pump divergence [full width at half maximum (FWHM) $1.18\sigma|\mathbf{a}(\varphi)|$] and the ring width under planar pumping (FWHM $0.089\bar{\theta}$). Instead of expressing this integral in terms of error functions, we have followed a numerical approach to solve this one-dimensional integral. As a good approximation we find that the relative increase in the (FWHM) ring width due to focused pumping depends on the angular position in the ring as

$$y(\varphi)=\sqrt{1+x(\varphi)^2}. \tag{5}$$

We note that Eq. (5) is a very good approximation; even the largest deviations (around $x=1$) between (FWHM) widths obtained from the numerically solved integral [Eq. (4)] and the approximation [Eq. (5)] are at most 5%. The asymmetric ring smearing is now directly quantified by Eq. (5) via the angle-dependent value $|\mathbf{a}|$. The top of the o-polarized ring ($\varphi=\pi/2$) remains narrow as $|\mathbf{a}|=1-1/\sqrt{2}\approx 0.29$ is small; at the bottom ($\varphi=-\pi/2$) the smearing is much larger as $|\mathbf{a}|=1+1/\sqrt{2}\approx 1.71$ is large; in between at $\varphi=0$ the smearing is proportional to $|\mathbf{a}|=\sqrt{1.5}\approx 1.22$. The simple Eq. (5) allows us to predict the ring width at a certain part of the ring, once we know the pump divergence σ and the ring width at plane-wave pumping.

If we repeat the above exercise for the e-polarized ring we find that the phase mismatch obeys the same Eq. (4) in the shifted radial coordinates of this ring. The e-polarized SPDC ring will therefore be simply a displaced version of the o-polarized ring, with identical shape and an "asymmetric smearing" in exactly the same orientation (narrow top, wide bottom).

The effect of focused pumping on coincidence imaging [9,10] can be calculated by performing a similar analysis as presented above. Instead of integrating over all angles $\boldsymbol{\theta}_e$ in Eq. (1), we can now fix $\boldsymbol{\theta}_e$ and simply calculate the integrand to obtain the coincidence image for the o polarization, and do the opposite for the e polarization. In the "thin-crystal limit," which is commonly applied [9,10], the phase mismatch is small at $\phi\approx 0$ and the coincidence image is just (a scaled version of) the pump profile $I(\boldsymbol{\theta}_p)$. Going beyond this limit, the phase-mismatch function will then also lead to asymmet-

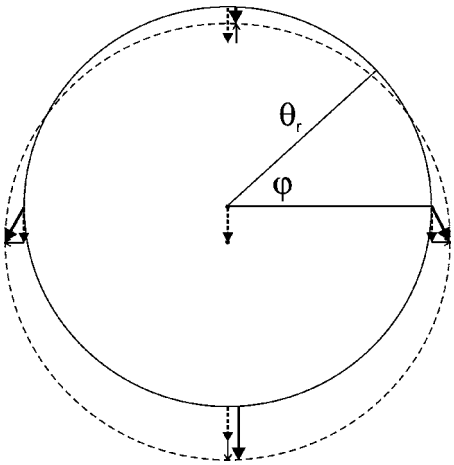

FIG. 1. The twofold effect of a change in the y component of the pump wave vector $\boldsymbol{\theta}_p$ on the SPDC ring: the center of the ring is shifted by $\theta_{p,y}$ (dotted arrow) while the radius of the ring increases by $\theta_{p,y}/\sqrt{2}$ (thin arrow). As the vector addition (thick arrow) of both effects depends on the angular position φ within the ring, the angular broadening due to focused pumping is nonuniform over the SPDC rings.

ric coincidence images for both polarizations. These coincidence images are only slices of the Gaussian pump profile, with a width and orientation that depend on the polarization and the angular position in the SPDC ring.

III. MEASUREMENTS AND RESULTS

The experimental setup is shown in Fig. 2. Light from a krypton ion laser operating at 407 nm is focused onto a 1 -mm-thick type-II beta-barium borate (BBO) crystal (cutting angle 41.2°), which was slightly tilted to generate orthogonal ring crossings (separated by $2\theta_{\text{off}}$). The focusing conditions of the pump light are varied by choosing different lens configurations before the crystal. A half-wave plate (HWP) and two 0.5-mm-thick compensating BBO crystals (labeled cc) compensate for the longitudinal and transverse walk-off of the SPDC light. Light emitted along the two orthogonal crossings of the SPDC cones passes apertures (for spatial selection) and $f=40$ cm lenses (L_1) at 80 cm from the generating crystal before being focused by $f=2.5$ cm lenses (L_2) onto free-space single-photon counters (Perkin Elmer SPCM-AQR-14). Polarizers (P) and interference filters (IFs, 10 nm spectral width) combined with red filters (RFs) are used for polarization and spectral bandwidth selection, respectively. Finally, the output signals of the photon counters are received by an electronic circuit that records coincidence counts within a time window of 1.76 ns.

In Fig. 3 we show the SPDC emission patterns for three different focusing conditions of the pump beam. These pictures were captured with an intensified charge-coupled device (CCD) (Princeton Instruments PI-MAX 512HQ) at 6 cm from the generating BBO crystal behind an interference filter (5 nm spectral width), a red plate, and two blue-coated mirrors that are needed to block the pump beam; no imaging lens was used. The three focusing conditions are

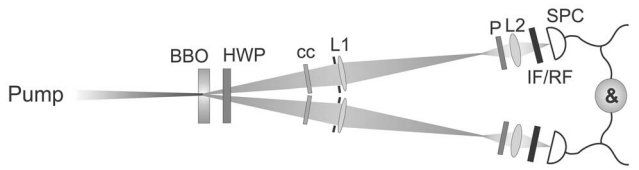

FIG. 2. Schematic view of the experimental setup (see text for details).

realized by choosing different lens configurations in front of the BBO crystal. For convenience, we will label these conditions as "plane wave," "intermediate," and "extreme," corresponding to a pump divergence σ of 0.86 ± 0.07, 12.0 ± 0.5, and 32 ± 1 mrad, respectively. These values were obtained by measuring the (far-field) pump size for the three focusing conditions using a CCD camera (Apogee AP1). For comparison, we note that the external offset angle $\theta_{\text{off}}\approx57$ mrad.

In the plane-wave case, our analysis of Fig. 3(a) yields a radial width of $\Delta\theta_r=10.9\pm0.5$ mrad (FWHM), being constant over the entire ring. However, this value is somewhat larger than the true width of the rings as broadening by the $\approx$0.4-mm-wide pump spot is still considerable at 6 cm from the crystal. At a BBO-CCD distance of 12 cm we obtained the better estimate of $\Delta\theta_r=8.8\pm0.5$ mrad; the same value was measured at larger distances [15]. The absence of asymmetric smearing, and thus the "plane-wave" condition, is not only supported by the measured constant ring width but also by the pump divergence of $\sigma=0.86$ mrad, for which Eq. (5) predicts a maximal normalized ring width (at bottom) of only $y=1.02$. Furthermore, the measured angular distance between the two crossings of $2\times(57\pm1)$ mrad is equal to the theoretical value of $2\theta_{\text{off}}$ (with $\theta_{\text{off}}=57$ mrad) that is needed for orthogonal ring crossings. The same value is used for the next two cases of focused pumping.

For intermediate focusing [see Figs. 3(b) and 3(d)] we clearly observe the theoretically expected asymmetric broadening of both rings: the measured radial width $\Delta\theta_r$ (FWHM) at the top, middle, and bottom of the rings was 8.3 ± 0.6, 17 ± 1, and 27 ± 1 mrad, respectively. These values are already true widths as we obtained approximately the same values at a BBO-CCD distance of 12 cm. We explain this by the less severe ring broadening by the much smaller pump spot in this case. By using the intermediate (FWHM) pump divergence of $1.18\sigma=14.2$ mrad and the measured (FWHM) ring width of 8.8 mrad in the plane-wave case, which combine to $x(\varphi)=|\mathbf{a}(\varphi)|\times14.2/8.8$, Eq. (5) predicts (FWHM) ring widths of 9.7 ± 0.9, 19 ± 2, and 26 ± 2 mrad at the three positions. Within the error margins, the measured values agree well with the predicted (FWHM) values.

The observation of the SPDC emission pattern under extreme focusing [see Fig. 3(c)] was limited by the aperture of the collection optics (dark edges) and the presence of extra (near-infrared) fluorescence that was not visible under weaker focusing conditions. The intensity of this fluorescence, which seems to originate from the BBO crystal, was measured to be roughly 4 times higher than the background intensity in the other focusing conditions, making its averaged intensity about 3.5 times higher than the SPDC intensity in the rings. The measured (FWHM) ring widths $\Delta\theta_r$ of

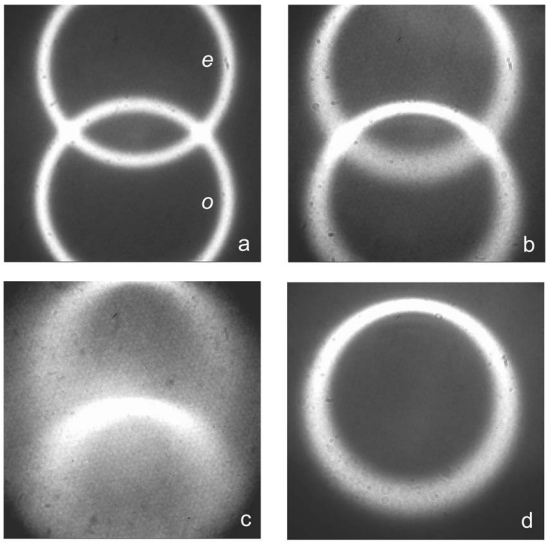

FIG. 3. SPDC emission patterns observed with an intensified CCD at 6 cm from a 1-mm-thick BBO, for three focusing conditions of the pump beam: (a) plane wave ($\sigma = 0.86 \pm 0.07$ mrad), (b) intermediate ($\sigma = 12.0 \pm 0.5$ mrad), and (c) extreme ($\sigma = 32 \pm 1$ mrad) with exposure times of 1, 1.3, and 0.8 s, respectively. In each of these pictures, the upper and lower rings correspond to extraordinary (e) and ordinary (o) photons, respectively. Picture (d) was taken behind a polarizer to highlight the ordinary ring in (b). All four images cover a space angle of 220 $\times 220$ mrad^2 and contain 100 accumulated snapshots.

10.8 ± 0.8, 48 ± 9, and 80 ± 15 mrad at the top, middle, and bottom of the ring, respectively, indeed reveal an even more severe and asymmetric broadening of the rings in comparison with the other focusing conditions. From the extreme pump divergence of $\sigma = 32$ mrad, we have calculated (FWHM) corresponding ring widths of 14 ± 1, 47 ± 4, and 65 ± 6 mrad, which match the measured widths within the error tolerances.

Next, we will compare the photon yield and entanglement quality of the polarization-entangled photon pairs that are generated under the three different focusing conditions. In Fig. 4 we show the measured single-count rate, quantum efficiency (=coincidence counts/single counts), and biphoton fringe visibility as a function of the aperture diameter. All measurements were performed in the 45°-polarization basis. Figure 4(a) shows how the single-count rate behind a relatively large 14-mm-diameter aperture drops from 800×10^3 s^{-1} in the plane-wave case (circles), to 70% of this value for intermediate focusing (triangles), and 60% under extreme focusing (squares). At smaller apertures the drop is even somewhat more pronounced. The relatively small difference between the intermediate and extreme cases is probably due to the excess fluorescence observed in the latter case. The drop in the single-count rate for stronger focusing is ascribed to the angular broadening of the ring crossings. The asymmetric character of this broadening creates an imbalance between the ordinary and extra-ordinary count rate at the crossings. In consistency with the SPDC patterns shown in Fig. 4, we measured about 5%, 40%, and 55% more ordinary than extraordinary photons for the plane-wave, intermediate, and extreme cases, respectively.

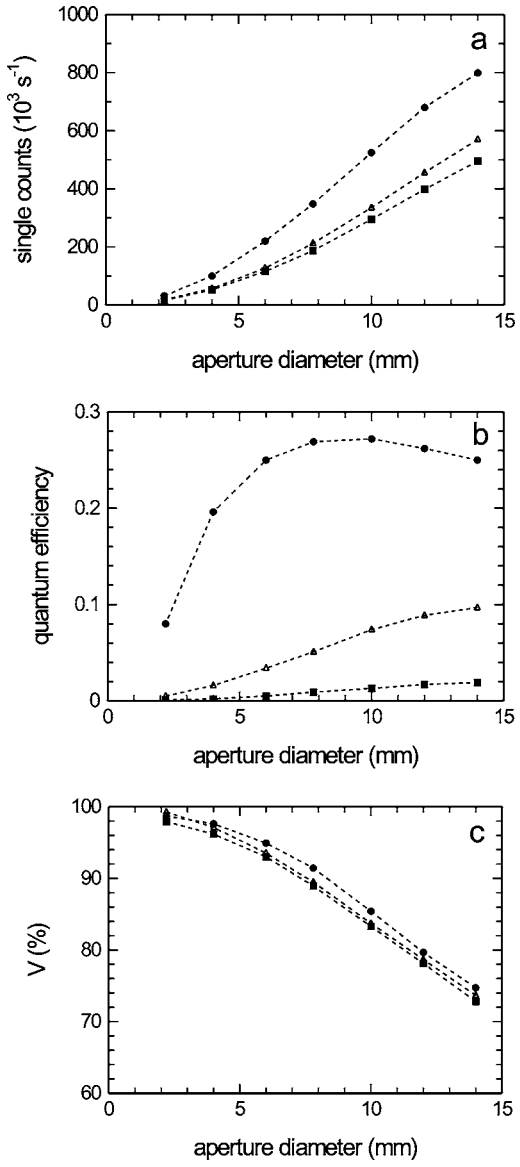

FIG. 4. Single-count rate (a), quantum efficiency (b), and polarization fringe visibility V (c) measured as a function of aperture diameter (at 80 cm from BBO crystal) for three focusing conditions of the pump: plane wave (dots), intermediate (triangles), and extreme (squares).

Figure 4(b) shows the quantum efficiency (=coincidence counts/single counts) as a function of aperture size. The maximum of 0.27 observed for plane-wave pumping is clearly much larger than the maxima observed for intermediate and extreme focusing, where we observed maxima of 0.10 and 0.02, respectively. Focused pumping thus leads to a much stronger reduction in the coincidence count rates than in the single count rates. Figure 4(b) also shows that the aperture diameter at which 50% of the maximum quantum efficiency is reached increases from ≈ 3 mm (=3.8 mrad) for the plane-wave case to 7.5 and 8.1 mm (≈ 10 mrad) for the intermediate and extreme cases, respectively, although the true maxima of the latter cases might not be reached yet. These numbers demonstrate the increase of the "transverse coherence area" of the down-converted beams, i.e., the an-

gular range in one beam that corresponds to a fixed angle in the other beam, as observable in coincidence imaging [9,10]. Focused pumping thus breaks the approximate one-to-one relation between the transverse positions of the twin photons observed under plane-wave pumping. This justifies the analogy to the transition from cw to broadband pumping where the exact anticorrelation in frequency between the two beams is destroyed [8].

Figure 4(c) shows the biphoton fringe visibility V, as measured by fixing one polarizer at 45° and rotating the other [3]. For plane-wave pumping, V decreases from $(98.7\pm0.2)\%$ at 2-mm-wide apertures to $(74.7\pm0.5)\%$ at 14 -mm-wide apertures. Virtually the same behavior is observed for both intermediate and extreme focusing, where the measured visibility is at most 2–3 % lower than in the plane-wave case. The entanglement quality is thus not drastically affected by focused pumping. On the other hand, although focused pumping produces wider rings and increased crossing areas, we apparently cannot profit from these increased areas due to a combined spatial-polarization labeling of the photon pairs. By reducing the aperture size we effectively remove this labeling and increase the entanglement quality, but this reduces the photon yield, the more so the stronger the focusing. For the considered geometry of bucket detectors behind apertures, focused pumping has no clear advantages. Mild focusing is expected to lead to a slightly increased yield in coincidence imaging [9,10].

We will end with a discussion of the effects of focused pumping on the optical spectrum, thus removing the restriction of narrowband spectral detection. For the geometry with bucket detectors behind small apertures the width of the optical spectrum is determined by the combination of the ring size and the "angular dispersion," i.e., the change in ring diameter with wavelength. Since the two ring sizes differ at the crossings due to asymmetric ring broadening, and since the angular dispersion is a material property [5], focused pumping should lead to different o and e spectra, and thus to spectrally labeled photons at the crossings. The same argument applies to the single-mode geometry based on fiber-coupled detectors. The focusing used by Kurtsiefer *et al.* [11] must have been just mild enough to miss the predicted effect. We predict that stronger focusing would have led to the mentioned spectral difference, thus enforcing the use of spectral filters in order to obtain a high polarization visibility.

A quick glance at Fig. 3 shows that the e ring is wider than the o ring at the crossing, making the e spectrum at this fixed collection angle wider than the o spectrum. Interestingly enough, the asymmetry in this type of spectral widening is just opposite from the spectral asymmetry predicted by Grice and Walmsley for pulsed pumping [8], where the o spectrum is wider than the e spectrum. Proper balancing of focused pumping and pulsed excitation could thus remove the spectral asymmetry and all spectral labeling.

IV. CONCLUDING DISCUSSION

We have investigated the effects of focused pumping on type-II SPDC. In particular, we have shown that focused pumping leads to an asymmetric broadening of both the SPDC emission cones. This is similar to asymmetric spectral broadening discussed in [8] for pulsed pumping or "focusing in time." For pair collection with two bucket detectors behind apertures, focused pumping seems to have no clear advantages; the polarization entanglement at fixed pinhole size is virtually unaffected, but the single- and especially the coincidence-count rates are reduced. For detection with fiber-coupled photon counters, where focused pumping is necessary for efficient single-mode generation, severe focusing is predicted to produce polarization-unbalanced spectral broadening that leads to a reduced entanglement quality.

ACKNOWLEDGMENTS

This work has been supported by the Stichting voor Fundamenteel Onderzoek der Materie; partial support is from the European Union under the IST-ATESIT contract.

[1] Z. Y. Ou and L. Mandel, Phys. Rev. Lett. **61**, 50 (1988).
[2] Y. H. Shih and C. O. Alley, Phys. Rev. Lett. **61**, 2921 (1988).
[3] P. G. Kwiat, K. Mattle, H. Weinfurter, A. Zeilinger, A. V. Sergienko, and Y. Shih, Phys. Rev. Lett. **75**, 4337 (1995).
[4] D. N. Klyshko, *Photons and Nonlinear Optics* (Gordon and Breach Science, New York, 1988).
[5] M. H. Rubin, D. N. Klyshko, Y. H. Shih, and A. V. Sergienko, Phys. Rev. A **50**, 5122 (1994).
[6] A. Joobeur, B. E. A. Saleh, and M. C. Teich, Phys. Rev. A **50**, 3349 (1994).
[7] T. E. Keller and M. H. Rubin, Phys. Rev. A **56**, 1534 (1997).
[8] W. P. Grice and I. A. Walmsley, Phys. Rev. A **56**, 1627 (1997).
[9] T. B. Pittman, D. V. Strekalov, D. N. Klyshko, M. H. Rubin, A. V. Sergienko, and Y. H. Shih, Phys. Rev. A **53**, 2804 (1996).
[10] C. H. Monken, P. H. Souto Ribeiro, and S. Padua, Phys. Rev. A **57**, 3123 (1998).
[11] C. Kurtsiefer, M. Oberparleiter, and H. Weinfurter, Phys. Rev. A **64**, 023802 (2001).
[12] F. A. Bovino, P. Varisco, A. M. Colla, G. Castagnoli, G. di Giuseppe, and A. V. Sergienko, Opt. Commun. **227**, 343 (2003).
[13] M. H. Rubin, Phys. Rev. A **54**, 5349 (1996).
[14] The phase mismatch is expressed by $\phi=\Delta k_z L/2$, where $\Delta k_z=k_{p,z}-k_{o,z}-k_{e,z}$. Equation (2), basically given in [13], is obtained by Taylor-expanding $k_{i,z}=n_i(\omega_i,\theta_{i,y}/n_i)\times(\omega_i/c)\cos(\theta_{i,x}/n_i)\cos(\theta_{i,y}/n_i)$ around the external angles $\theta_{i,x}=\theta_{i,y}=0$, using $\partial n/\partial\theta_{y,\mathrm{ext}}=\rho$ for the extraordinary rays.
[15] P. S. K. Lee, M. P. van Exter, and J. P. Woerdman, Phys. Rev. A **70**, 043818 (2004).